Theory of Deformable Substrates for Cell Motility Studies

Mark A. Peterson
Mount Holyoke College, South Hadley, Massachusetts 01075 USA

ABSTRACT Linear theory is used to relate the tractions F applied by a cell to the resulting deformation of fluid, viscoelastic, or solid substrates. The theory is used to fit data in which the motion of a fluid surface in the neighborhood of a motile keratocyte is visualized with the aid of embedded beads. The data are best fit by modeling the surface layer as a two-dimensional, nearly incompressible fluid. The data favor this model over another plausible model, the planar free boundary of a three-dimensional fluid. In the resulting diagrams for the distribution of F, it is found that both curl F and div F are concentrated in the lateral extrema of the lamellipodium. In a second investigation, a nonlinear theory of weak wrinkles in a solid substrate is proposed. The in-plane stress tensor plays the role of a metric. Compression wrinkles are found in regions where this metric is negative definite. Tension wrinkles arise, in linear approximation, at points on the boundary between positive definite and indefinite regions, and are conjectured to be stabilized by nonlinear effects. Data for the wrinkles that would be produced by keratocyte traction are computed, and these agree qualitatively with observed keratocyte wrinkles.

INTRODUCTION

Albert Harris (Harris et al., 1980) has described wrinkles generated in a thin rubber substrate by living cells. The wrinkles reveal the tractions exerted by cells on the substrate, but only indirectly. The wrinkles are suggestive, but no quantitative theory of this nonlinear phenomenon is available that has been found to be useful in this context.

It is known, however, that there is a nonzero threshhold for wrinkling, and that for sufficiently small in-plane stresses the response will also be in plane (see A Theory of Harris Wrinkles, below). In this regime the response should be linear and analysis straightforward. Recently Tim Oliver and Ken Jacobson observed this regime, visualizing the in-plane displacements by the movement of latex beads embedded in the silicone rubber sheet (Oliver et al., 1993, 1994). They have used linear elasticity theory to deduce the tractions produced by motile keratocytes on such sheets (Dembo et al., 1996). The cross-linked substrates suitable for this analysis, however, had a shear modulus sufficiently large that the resulting bead displacements were small and difficult to measure.

In this paper it is suggested that fluid substrates are also suitable for such experiments and have the advantage of giving much larger displacements to applied tractions. For linear theory to apply it is no longer necessary that displacements be small, only that they be slow. Oliver and Jacobson observed such substrates in earlier experiments, but never analyzed them quantitatively. I analyze some of their fluid substrate data, assuming that the surface behaves as a two-dimensional fluid, and show that the traction pattern agrees with the pattern they found on a solid substrate (Dembo et al., 1996). The larger displacements in the fluid substrate, however, mean that the pattern is determined with higher accuracy. (Of course it is possible that the pattern of tractions really depends on the substrate, as the cell adjusts its behavior to its environment, but the similarity between these two independent determinations of traction is suggestive.) The details of the two-dimensional fluid model are in Appendix A.

The possibility that the substrate was not a simple fluid but rather a viscoelastic material was checked by considering a one-parameter family of models that interpolate between simple fluid at one extreme and elastic solid at the other, parameterized by a memory time. The memory time is zero in a simple fluid and infinite in an elastic solid. The goodness of fit to the model improves as the memory time decreases, down to the shortest time that the measurement can resolve. That is, the data are best explained by the model with no elasticity at all, the simple fluid. If it is possible to produce truly viscoelastic films, however, the more general model developed here might be useful in analyzing them. The viscoelastic model is described in Appendix B.

The two-dimensional fluid model is motivated by the preparation method for the substrate layer, going back to Harris et al. (1980). The free boundary of a silicone fluid is briefly heated; if cross-linking is not achieved, because of insufficient heating, it is still assumed that a thin layer of higher viscosity is formed, and that the internal forces within this thin layer will be more important than forces from adjoining material, as is surely true in the fully cross-linked substrate. This can actually be checked. It is easy to elaborate the two-dimensional model to include the effect of the adjoining material, with an independent parameter to govern the strength of the coupling. This amounts to a one-parameter family of models that interpolate between the two-dimensional fluid and a model that might seem more

Received for publication 5 March 1996 and in final form 8 May 1996.

Address reprint requests to Dr. Mark A. Peterson, Physics Department, Mount Holyoke College, South Hadley, MA 01075. Tel.: 413-538-2525; FAx: 413-538-2239; E-mail: mpeterso@mtholyoke.edu.

0006-3495/96/08/657/13 $2.00

natural, the surface layer as the mathematical boundary of a three-dimensional isotropic fluid. Within this family the two-dimensional fluid still gives the best fit to data. These models are described in Appendix C.

If it is true, as it appears, that the surface layer behaves like a two-dimensional fluid, it may be because the heat treatment has created a thin layer with its own mechanical integrity, and with a large viscosity that dominates the dynamics. It also appears possible, although there is certainly no compelling reason to believe it, that normal fluid surfaces, even without such treatment, might respond to gentle perturbations in a two-dimensional way. The regime visualized in this experiment, in which very small tractions are applied to a free surface, has perhaps not been very much studied. Familiar phenomena like surface tension accustom us to regard free fluid surfaces as more than simply mathematical boundaries—they have their own proper physical characteristics. It is at least conceivable that free surfaces have their own mechanical integrity that small perturbations do not immediately disrupt. For some purposes one can model surface tension as the effect of a thin elastic membrane at the free surface of a fluid; the idea suggested here (tentatively, and strictly as an aside) would ascribe even more reality to this membrane than is usual. A peculiarly two-dimensional response to traction would show up as having a longer range than the response in a simple three-dimensional fluid. That is presumably what lies behind the consistently better fit to two-dimensional models in this experiment (where there is a much less speculative reason to expect two-dimensional behavior). The data seem to exhibit a longer range response to traction than the three-dimensional model predicts. It should be said, in the end, that the pattern of traction that emerges is actually very similar for both two- and three-dimensional models. The pattern of traction is thus a fairly robust result and does not depend crucially on the two-dimensional model.

Because the tractions exerted by keratocytes are now well characterized, and because keratocytes have been observed to produce weak wrinkles on solid substrates, it is of interest to attempt a quantitative theory of wrinkles in this case. The last section of the paper takes a first step in this direction, with an infinitesimal stability theory approach. It describes in linear approximation the regions where a keratocyte developing small tractions could begin to produce weak wrinkles in a solid substrate. According to this weak wrinkle theory, the keratocyte traction should produce wrinkles that are qualitatively like those that have been observed. This is additional evidence for the correctness of the keratocyte traction pattern found in Dembo et al. (1996) and the first sections of this paper. The infinitesimal weak wrinkle theory given here complements a long-known wrinkle theory called tension field theory, which describes the opposite extreme, strong wrinkles due to large anisotropic tension. The relationship of these two wrinkle theories is described.

IN-PLANE MOTIONS

I model the substrate layer as a two-dimensional compressible Newtonian fluid. Appendix B describes a more general model, in which the layer is viscoelastic, but the best fits to data are for this model, which is also the simplest. Of course, the fluid layer is incompressible in a three-dimensional sense, but this does not constrain the surface to appear incompressible, hence the inclusion of compressibility in the model. With the assumption of two-dimensionality, the model is a consequence of the same phenomenological arguments that lead to the equations of motion of any fluid. The effect of coupling to the bulk fluid, including the other extreme, that the surface layer is simply the surface of a three-dimensional isotropic fluid, is considered in Appendix C. Again, these more general models do not lead to better agreement with data.

Inertial effects are negligible at the slow time scales of these cell experiments, so the fluid may be considered to be always in mechanical equilibrium.

If $\vec{v}(\vec{r})$ is the in-plane velocity of an isotropic two-dimensional fluid, then the associated stress tensor, in Cartesian coordinates, is (Landau and Lifshitz, 1959)

$$S_{ij} = \kappa v_{k,k}\delta_{ij} + \eta(v_{i,j} + v_{j,i}), \tag{1}$$

where κ and η are two-dimensional viscosities. In particular, κ is a two-dimensional "bulk viscosity," associated with area changes, and η is the shear viscosity.

The mechanical equilibrium of the fluid is expressed by

$$S_{ij,j} = -F_i^{ext}, \tag{2}$$

where $\vec{F}^{ext}$ is the force per unit area applied to the substrate by the cell in the contact area D. Equation 2 is a classical partial differential equation for $\vec{v}$. As in other two-dimensional flow problems, the introduction of complex variables gives an efficient solution. This method (Timoshenko and Goodier, 1951) is described in Appendix A. The Green's function solution to Eq. 2 is

$$v(z) = -\frac{1}{4\pi\eta}\int\int_D \left[\left(\frac{\kappa+3\eta}{\kappa+2\eta}\right)F\ln|z-w| + i\left(\frac{\kappa+\eta}{\kappa+2\eta}\right)\frac{\mathrm{Im}[F(\bar{z}-\bar{w})]}{\bar{z}-\bar{w}}\right]dA_w, \tag{3}$$

where the integral goes over the region D in which the applied force is nonzero, i.e., the contact area of the cell. In Eq. 3 the various 2-vectors are represented as complex scalars according to the usual identification

$$z = x + iy, \quad v = v_x + iv_y, \quad F = F_x^{ext} + iF_y^{ext}, \tag{4}$$

that is, x and y components of 2-vectors become real and imaginary parts of complex numbers. The solution is identical to that given by Lamb (1932), in the incompressible

case $\kappa \to \infty$; Lamb also points out that the solution behaves badly at infinity unless

$$\int_D F \, dA_w = 0 \tag{5}$$

a condition that is of course satisfied here, because the net force on the cell due to the substrate is zero to excellent approximation.

DATA ANALYSIS

In this section I use the result of the previous section to analyze tractions imposed by a motile keratocyte on a fluid substrate. As described by Oliver et al. (1993), the data consist of a sequence of digitized video frames, taken every 2 s, of a keratocyte moving with essentially uniform velocity (about 12 μm/min) in a direction I take as the x axis. There are over 100 latex beads visible in these pictures, embedded in the substrate. I analyzed their motion as follows. I selected a sequence of 10 frames, uniformly spaced in time, at an interval $\Delta t = 40$ s, and in each of these frames digitized the positions b_{ij} (ith frame, jth bead) of each of 95 beads, to an accuracy of better than 1 pixel. I also digitized a sequence of points around the cell outline in each picture. The outline did not change shape very significantly during the sequence. Finally, I digitized the location o_i, in each frame ($i = 1$–10) of an organelle visible in the cell body that seemed to keep a fairly fixed position relative to the rest of the cell. Translating the data for each frame to bring o_i, to the origin gives bead positions

$$B_{ij} = b_{ij} - o_i, \tag{6}$$

as measured from a fixed point in the cell. The tracks B_{ij} are graphed in Fig. 1, with the average cell shape also indicated. Because o_i, is not an unambiguous position, B_{ij} has a small systematic error associated with each i (each frame). This shows up as a slight waviness in the tracks of the beads. The cell is moving from left to right in the original sequence, but here one must imagine the cell as fixed, and the beads as moving from right to left. One has the impression of a steady flow that is perturbed by the cell.

Because the flow in Fig. 1 appears steady, the time-dependent velocity V of the substrate in the laboratory frame has the form

$$V(x, y, t) = v(x - v_0 t, y), \tag{7}$$

where v_0 is the constant speed of the cell, and the function $v(x, y)$ is a steady flow velocity in the cell frame, due to an assumed constant distribution of force F. This steady flow pattern is something one can construct from the bead positions. One can then fit this information by choice of F in Eq. 3, and so get information on the force exerted by the cell.

The beads give one a table of 855 complex values for the steady velocity v^{ij}, each assigned to a midpoint position z^{ij}, ($i = 1$–9, $j = 1$–95):

$$v^{ij} = \frac{b_{i+1j} - b_{ij}}{\Delta t} \tag{8}$$

$$z^{ij} = \frac{B_{i+1j} + B_{ij}}{2} \tag{9}$$

These data are shown graphically in Fig. 2. The systematic error in B_{ij} pointed out after Eq. 6 becomes a small systematic error in the assigned positions z_{ij}. The velocity vectors

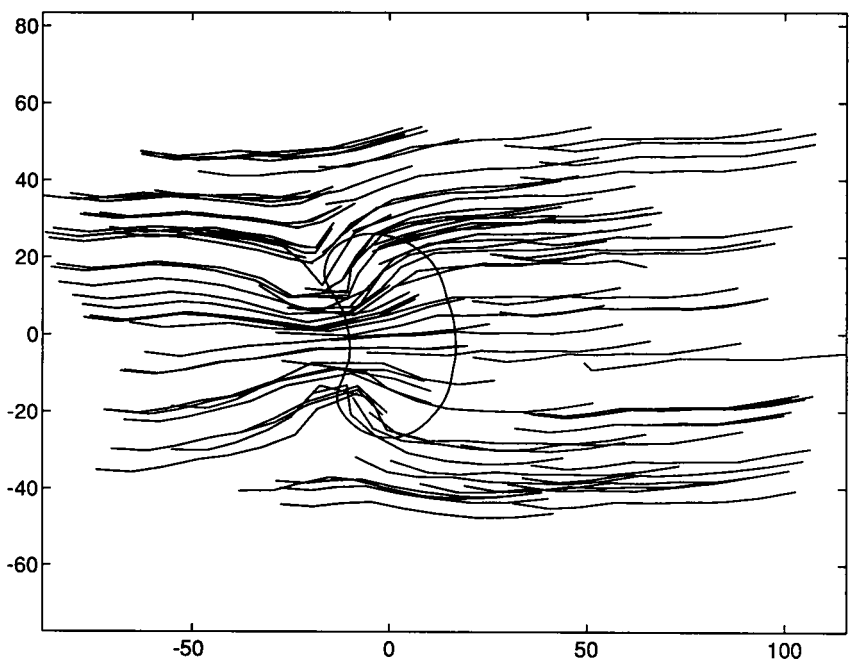

FIGURE 1 The tracks of individual beads are shown in the cell rest frame. The beads move from right to left in this view, corresponding to the motion of the cell in the laboratory frame from left to right. The average stationary cell outline is also shown. Numbers on axes are coordinates in microns.

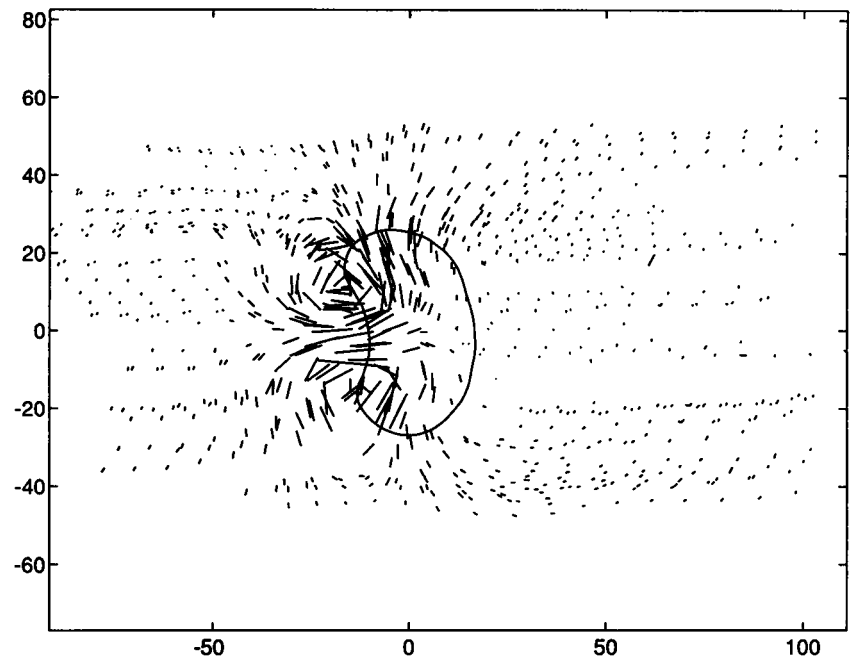

FIGURE 2 The velocities of individual beads are shown in the laboratory frame, assigned to their mean position with respect to the cell during the interval the velocity was determined. Each bead determines a velocity at nine different relative positions because of the motion of the cell and the way the data were sampled. The sense of the velocity vectors (not indicated to avoid clutter) can be inferred from Figs. 1, 3, and 4.

v_{ij} themselves, however, do not have this error. They are as accurate as the raw data. Thus Fig. 2 gives a more accurate picture of how the beads actually move than Fig. 1 does, even allowing for the change in reference frame.

The problem is to choose F within the cell outline to fit the data in Fig. 2.

I use an inverse Monte Carlo technique. If F were known and one were to evaluate the integral in Eq. 3 by a Monte Carlo method, one would select many points w randomly within the cell outline, evaluate the integrand at each one, add the results, and scale appropriately. In the inverse method one selects points w randomly, does the evaluation for each z^{ij}, but leaves it open what values will be taken for F, then finally chooses F to minimize the mean square deviation from the known values v^{ij}. This produces values F at random points w in the cell. One gets a feeling for the distribution of F and the consistency of the method by repeating this process. F is quite consistent from one trial to the next.

The goodness of fit can be determined by finding the root mean square deviation of the fitted v^{ij}'s from the data. I am considering a family of fluid models, parameterized by the viscosities κ and η. The best model, in the sense of the best fit, is for

$$\kappa/\eta \approx 20 \tag{10}$$

(an overall scale factor is unknown, because the substrate is not calibrated). The rather large ratio of bulk viscosity κ to shear viscosity η means the two-dimensional fluid is almost incompressible (in the two-dimensional sense). This model was used for the remaining computations in this section.

After repeated fittings one has an estimate of the applied force at many points in the cell. Using these, one can assign a force to any point in the cell by averaging the fit values at nearby points, weighting the closest points more heavily (I used a Gaussian weighting function with a characteristic width less than the minimum distance between points in any one fit). This averaging also smooths out the probabilistic fluctuations present in each fit individually. The result is very accurately reproducible. Fig. 3 shows the force calculated in this way at 80 random points, 40 in the interior of the cell and 40 on the edge. Fig. 3 confirms the pattern found by Dembo et al. (1996) in all essential respects, but because of the improved signal-to-noise in the raw data shows a higher level of detail. The same pattern appears in each half of the cell, although no requirement of symmetry is built into the procedure. (A second cell, moving similarly, on a similar substrate, showed a virtually identical traction pattern.)

The net F, found by summing the F's in any one fit, or in principle integrating over the contact area D, should of course be zero. This is sure to be approximately true in the fitting procedure, even if it is not imposed as a constraint, because, as pointed out after Eq. 5, otherwise the computed v's will not go to zero at large distances from the cell, and in the data there are many points at large distance, all with very small v. Thus it is no surprise that in an unconstrained fit, $\Sigma F \approx 0$. I have also done all the fits with the constraint that $\Sigma F = 0$, using a Lagrange multiplier method. There is no appreciable difference in the outcome of any quantity when one uses this constrained fitting procedure. The results reported below were obtained with unconstrained fits.

F computed in this way, using random points, averaging, etc., is of course a random variable, but because I use many fits, and the individual fits are very consistent with each other, the random component in the computed F is small enough that meaningful numerical derivatives of F can be computed. Because F is a vector field, the natural deriva-

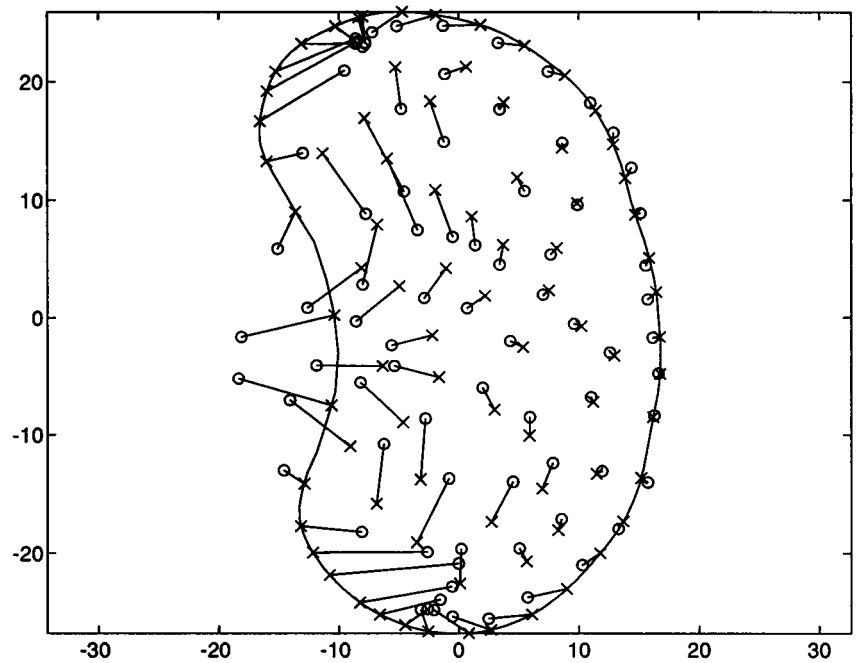

FIGURE 3 The force F exerted by the cell on the substrate is shown at 80 random points labeled x. Each force is in the direction of the corresponding o.

tives are the divergence and curl, shown in contour maps in Figs. 4 and 5.

The curl of the force seems to be concentrated in four principal regions in Fig. 4, which one might call "force vortices," because the force rotates within them like the velocity vector in a flow vortex. Each represents a region where the cell applies a torque to the substrate. The sense of the torque alternates as one moves around the cell from one region to the next, that is, the force vortices tend to counterrotate like meshed gears. The net torque exerted by the cell as a whole must be zero, of course, so a force vortex cannot exist in isolation.

The divergence is negative, and concentrated in two lateral areas in the lamellipodium, and is closely associated with the lateral regions of nonzero curl, as shown in Fig. 5. In this region the force applied by the cell tends to compress the substrate, in what one might call a "force sink." The sinks occur right between the vortices.

Both divergence and curl are concentrated in the lateral extrema of the lamellipodium. Even without knowing the

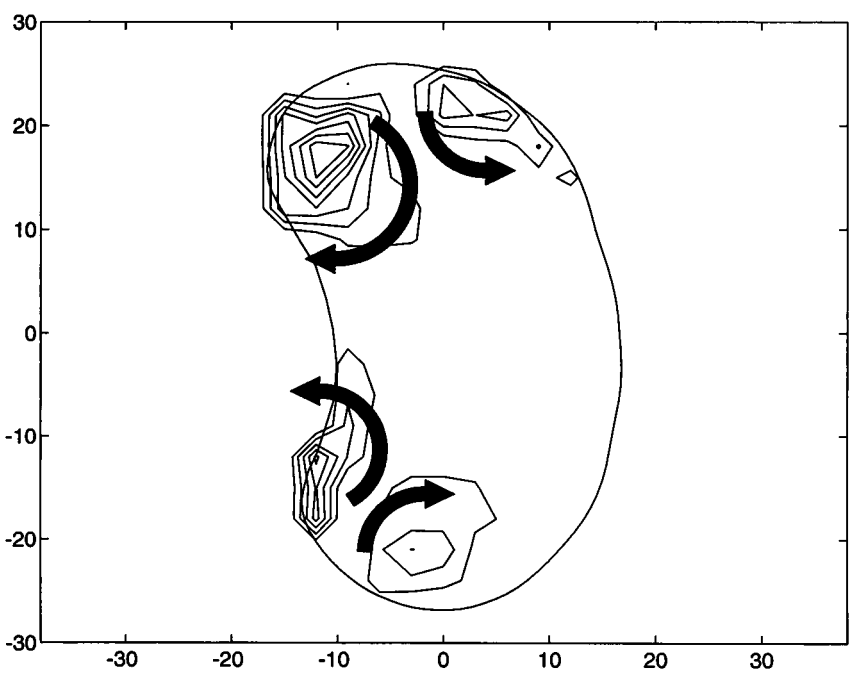

FIGURE 4 Curl F is shown in a contour plot. The sense of rotation in each of four "force vortices" is indicated by arrows. The sense alternates as one moves from one vortex to the next. The same alternating sense of rotation of F can be understood by comparison with Fig. 3. The force vortices coincide fairly well with the lamellipodium, except that the leading edge of the lamellipodium, on the right half of the cell outline, is free of them. The rear vortices are stronger than the leading ones.

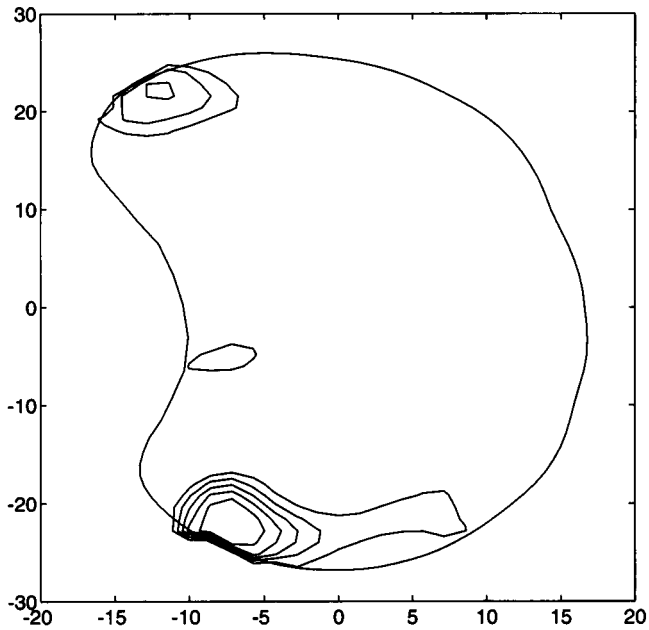

FIGURE 5 Div F is shown in a contour plot. The divergence is negative and concentrated mainly in regions between the force vortices of Fig. 4. The force exerted by the cell tends to compress these regions.

mechanism, one can be quite sure that some mechanism shaping the pattern of force generation is operating in these regions. Outside these regions F is approximately a harmonic vector field, which is simply the smoothest interpolation between one region and another. This suggests that the rest of the cell, from the point of view of force generation, conforms more passively to these obviously active regions. From the standpoint of mathematics it is natural to say that the force pattern is determined in those regions where the divergence and curl are appreciable, that is, in the lateral lamellipodium. It will be interesting to know, when the mechanism for the production of this force is understood, whether the biology agrees with this mathematical hint.

It has been observed that fragments of lamellipodium can crawl autonomously, mimicking a whole cell (Euteneuer and Schliwa, 1984; see sequence in Fink, 1995, filmed by Mark Cooper). It would be interesting to know if such fragments also contain a pair of force vortices, and if motility in keratocytes is always associated with this pattern of force. It is of course possible that the forces responsible for motility, which could be much smaller than the forces that are visualized in this experiment, are quite independent of the phenomenon seen here, and that this pattern of force has more to do with anchoring the cell than with moving it, for instance. Observations of motile fragments on a fluid substrate could help to answer this question.

A THEORY OF HARRIS WRINKLES

I turn now to the question of interpreting the weak wrinkles produced by cells in solid substrates. The observations here are still of a preliminary character, but they provide a kind of corroboration of the keratocyte traction pattern found in the analysis of fluid substrates, and so, in a sense, represent a semiquantitative interpretation of wrinkles. I point out the difference between compression wrinkles and tension wrinkles, and how these ideas complement tension field theory (Mansfield, 1969; Reissner, 1938; Wagner, 1929), a theory of strong wrinkles.

If a solid substrate film wrinkles, it is because it can thereby lower its elastic energy. Consider a two-dimensional solid with Lamé constants μ and λ, representing a fully cross-linked thin silicone rubber substrate; let $\vec{u}$ be the in-plane displacement, and let w be the displacement normal to the x-y plane, both regarded as functions of x and y. The strain tensor, to lowest nontrivial order in $\vec{u}$ and w, is (Landau and Lifshitz, 1959)

$$\sigma_{ij} = \frac{1}{2}(u_{i,j} + u_{j,i} + w_{,i}w_{,j}), \tag{11}$$

and the elastic energy is

$$E = \iint_D \left[\frac{K}{2}(\nabla^2 w)^2 + \frac{\lambda}{2}(\sigma_{ii})^2 + \mu\sigma^{ij}\sigma_{ij}\right] dA. \tag{12}$$

The first term is the curvature energy, with coefficient the bending modulus K. Repeating for the most part the above conventions (see In-Plane Motions), let $u(z)$ be the in-plane displacement at position z. The equilibrium response to force F in the absence of wrinkling is

$$u(z) = -\frac{1}{4\pi\mu}\iint_D \left[\frac{\lambda + 3\mu}{\lambda + 2\mu} F \ln|z - z'| + i\frac{\lambda + \mu}{\lambda + 2\mu}\frac{\mathrm{Im}[F(\bar{z} - \bar{z}')]}{\bar{z} - \bar{z}'}\right] dA', \tag{13}$$

just the analog of Eq. 3 for an elastic solid. Now imagine that, for fixed force F and in-plane displacement u, the substrate is allowed to move normal to itself by an amount $w(z)$. Can it thereby lower its energy? This is the question of stability against buckling. Because in-plane strain σ depends on w only in second order, the stress tensor

$$S_{ij} = \lambda u_{k,k}\delta_{ij} + \mu(u_{i,j} + u_{j,i}) \tag{14}$$

can be considered constant in a lowest order theory. The part of the energy that depends on w is

$$E = \frac{1}{2}\iint_D \left[K(\nabla^2 w)^2 + S_{ij}w_{,i}w_{,j} + \frac{\lambda + 2\mu}{4}|\vec{\nabla}w|^4\right] dA. \tag{15}$$

The variational condition that E be minimal with respect to variations of w is

$$K\nabla^2\nabla^2 w - \left[S_{ij}w_{,ij} - F_j^{ext}w_{,j} + \left(\frac{\lambda}{2} + \mu\right)(w_{,i}w_{,j}w_{,i})_{,j}\right] = 0 \tag{16}$$

I have used the fact that

$$S_{ij,i} = -F_j^{ext} \tag{17}$$

in equilibrium.

Qualitatively, one notes that the curvature energy, the term with coefficient K in Eq. 15, is nonnegative, and in fact positive definite for a sample of finite size. Any lowering of the energy must therefore come from the second term, involving the stress tensor. But the stress tensor is linear in F. Hence for sufficiently small F the positive curvature energy dominates, and the film is infinitesimally stable against buckling. The argument goes back to Euler.

The surprising thing about wrinkles is that they have one large principal curvature, almost by definition, in spite of the fact that this obviously costs curvature energy. Curvature seems to be not so relevant in a wrinkle solution. This suggests that one might find singular wrinkle solutions by ignoring the curvature energy altogether, invoking it only to prevent the curvature from becoming infinite. That is, one thinks of the curvature energy as perturbing the wrinkle solution associated with F rather than F as perturbing a solution dominated by curvature energy.

Without K the equilibrium condition becomes

$$S_{ij}w_{,ij} - F_j^{ext}w_{,j} + \left(\frac{\lambda}{2} + \mu\right)\nabla^2 w|\vec{\nabla}w|^2 + (\lambda + 2\mu)w_{,ij}w_{,i}w_{,j} = 0. \tag{18}$$

This is a second-order quasilinear equation in two independent variables, for which there exists a very extensive theory (Courant and Hilbert, 1962). The crucial ingredient in the theory is the notion of characteristic curve. For a quasilinear equation the characteristic curves cannot be computed once and for all, but rather depend on the particular solution one has in mind. However, if one is interested particularly in wrinkle solutions, one may note that wrinkles physically do not suddenly appear at nonzero amplitude. Rather, they seem capable of bifurcating smoothly from the flat solution. Therefore one should look at the linearized version, regarded as a guide to infinitesimal buckling instability,

$$S_{ij}w_{,ij} - F_j^{ext}w_{,j} = 0 \tag{19}$$

For this linear equation the characteristics can be computed once and for all. They depend entirely on the in-plane stress tensor S, Eq. 14, which plays the role of a metric. In particular, if S is indefinite, like the Lorentz metric, then there are real characteristics, and the equation is hyperbolic. In this case the partial differential equation requires disturbances to propagate along the bicharacteristics: there are two characteristic directions at each point. (This propagation is not "in time," of course; rather, the static solution can be generated in this way.) If S is definite, on the other hand, there are no real characteristics, and the solution cannot be thought of as "propagated." The equation is elliptic.

The actual situation is more complicated and more interesting than either of these possibilities. The "stress geometry" realizes both possibilities, in different regions. The equation is hyperbolic in some places, elliptic in others. The elliptic regions fall into two types, type P, where S is positive definite, and type N, where S is negative definite. Buckling is energetically unfavorable in P regions and favorable in N regions. Thus we would expect buckling in N regions. These buckled N regions appear to be nothing other than compression wrinkles.

A third type of point also arises, on the boundary curves between hyperbolic and elliptic regions, the parabolic points. At a parabolic point the two characteristic directions degenerate to a single direction. Characteristics from the hyperbolic side of the parabolic curve come into parabolic points tangent to each other, and end. (The Tricomi equation is a much studied example of this (Garabedian, 1964).)

I propose that tension wrinkles are initiated at parabolic points where the tension direction is tangent to a parabolic curve. The justification for this idea is as much physical as mathematical. Because tension wrinkles are well localized, there must be some reason why the disturbance they represent does not smoothly propagate over the entire hyperbolic region. The parabolic points on the boundary of a P region (P-parabolic points) represent a barrier to such propagation, because the P region itself must be flat. One can think of a disturbance that is propagated as far as the P region as being trapped against the "wall" of P-parabolic points, able to propagate no farther. If the tension direction happens to be aligned tangent to the curve of P-parabolic points, then tension can do nothing to inhibit the formation of a wrinkle (as it could if it had a component perpendicular to the wrinkle, able to pull the wrinkle flat).

A little more detail is helpful in explaining this suggestion. At parabolic points S has a zero eigenvalue (this characterizes the parabolic points). At hyperbolic points the eigenvectors of S and the characteristic directions for Eq. 19 have no simple relationship, but at a parabolic point the unique characteristic direction coincides with one eigenvector of S, the one belonging to the nonzero eigenvalue. At a P-parabolic point this is what I called the tension direction in the paragraph above, belonging to a positive eigenvalue of the stress tensor. Thus the characteristic direction should be tangent to the P-parabolic curve. This condition will be met only at isolated points, generically speaking, but at these points disturbances may grow. Then, I suggest, the nonlinear terms stabilize the new wrinkled configuration and allow it to extend along the local tension direction.

A simple test of these ideas is the wrinkle pattern generated by a force applied at one point; one can, for example, scald milk to form a thin solid film on the surface, then stress it with a needle. V-shaped wrinkles form behind the needle. In the theory, with the solid assumed incompressible, the stress tensor due to a force F applied at the origin

0 has a zero eigenvalue at every point (this is a very degenerate case). That is, all points are parabolic points. They are P-parabolic behind the needle, and N-parabolic in front of the needle, if we name them by the sign of the nonzero eigenvalue. The characteristic directions are radial and centered on 0, so that the tension directions are exactly the rays extending behind the needle from 0, agreeing with the observed wrinkles. The computation is in Appendix D.

The above example of force applied at a point recalls the ideas of "tension field theory" (Mansfield, 1969; Reissner, 1938; Wagner, 1929). This is a theory of wrinkles valid in the limit of large stress. Its starting point is the idea that under some circumstances the stress is so large and so anisotropic that one eigenvalue of stress is negligible compared to the other: in effect, that the parabolic points form not curves, but regions, as they rather accidentally do, even for small applied force, in the case of stress applied at one point to an incompressible membrane. In tension field theory the problem is to find the tension lines in these parabolic regions. It is a principal result in this limiting case that the lines are straight, like the V-shaped wrinkles in the example. These tension lines are the candidate wrinkles of the theory. Instead of isolated points where the tension direction is tangent to a P-parabolic curve, there are whole families of integral curves of the tension field consisting entirely of P-parabolic points.

It is clear that the weak wrinkle theory suggested here represents as much of tension field theory as one can build into a linear theory with general stress tensor. That is perhaps its best justification. It seems plausible that the effect of the nonlinear terms of the more general theory would be to interpolate between the two theories, i.e., once tension wrinkles are nucleated at a P-parabolic point, their effect on the stress tensor is to promote the development of more P-parabolic points along curves tangent to the tension direction until, in some limit of very large stress, all points have this character. I have not shown this, but I suggest it as a plausible scenario.

A computed example is interesting in this regard. Fig. 6 shows data for the stress that would be produced in an incompressible substrate by the forces in Fig. 3. There is a large N region, blank except for the label N. There are two small P regions at the rear of the cell, labelled and contoured in an attempt to make them visible. The remaining region is hyperbolic, with the eigenvector corresponding to the positive eigenvalue of stress indicated: the length of the line indicating direction is chosen proportional to the magnitude of the eigenvalue, to indicate the strength of the tension as well. As one approaches a P-parabolic point, this direction approaches the tension direction (characteristic direction). As one approaches an N-parabolic point, the positive eigenvalue goes to zero, and the line goes toward zero length. One sees at the lateral extrema of the cell that the tension does not always seem to approach zero at the boundary, even though according to the labeling, these should be N-parabolic points. Apparently there are small P-regions there, too small to be resolved by the contouring routine. (The stress is rapidly varying there.) According to the ideas above, there could be a large broad compression wrinkle along the symmetry axis of the cell, and tension wrinkles could be nucleated at isolated P-parabolic points (on the boundaries of the elliptic regions where the tension does not approach zero).

Both major features suggested in Fig. 6 have been observed. In undergraduate thesis work (Lasic, 1994) at Mount Holyoke College, Morana Lasic obtained video micrographs of keratocytes on silicone rubber which show tension wrinkles emanating from the lateral extremities of the cell, as seen in Fig. 7. I suggest that these wrinkles were initiated at P-parabolic points on the

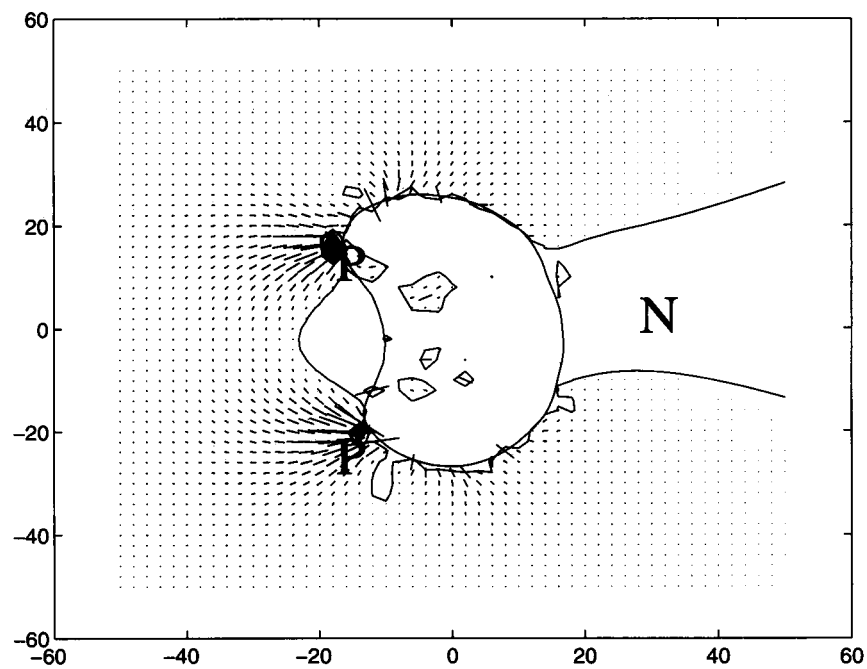

FIGURE 6 This figure shows the features of the stress geometry relevant to the formation of wrinkles for the force F in Fig. 3. Elliptic regions of the governing differential equation are labeled P or N, depending on whether S is positive or negative definite. The two small P regions are contoured. In hyperbolic regions the direction of the positive eigenvector of stress S is shown at selected grid points, with length proportional to the eigenvalue. This eigenvalue goes to zero on the boundary of an N region. That it appears not to do this at the lateral extrema of the cell means that the stress is rapidly varying there, and there may be small P regions there that were too small to outline with contours. The cell could have a compression wrinkle in the large N region, and tension wrinkles could nucleate on the boundaries of P regions.

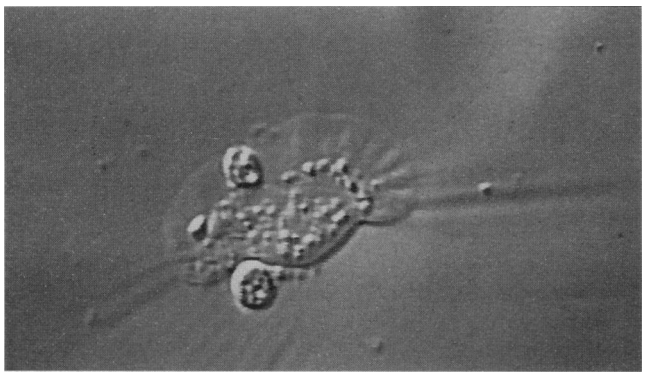

FIGURE 7 Photograph of a keratocyte on silicone rubber taken by Morana Lasic (unpublished senior thesis, Mount Holyoke College). The observed wrinkles are where Fig. 6 predicts tension wrinkles could be initiated.

boundary of the elliptic regions seen in Fig. 6. Once the wrinkles were initiated, nonlinear terms became important and stabilized them. Compression wrinkles that go through the keratocyte roughly parallel to the direction of motion seem to be typical, according to Dembo et al. (1996). This feature is like the N region in Fig. 6.

APPENDICES

A: Two-dimensional fluid model

Following classical methods (Timoshenko and Goodier, 1951; Schutz, 1980), I solve the equation for the velocity v of a two-dimensional fluid with viscosities η and κ,

$$S_{ij,j} = -F_i^{ext}, \tag{20}$$

where the stress tensor S_{ij} is given by

$$S_{ij} = \kappa v_{k,k} g_{ij} + 2\eta \dot{\sigma}_{ij} \tag{21}$$

$$\dot{\sigma}_{ij} = \frac{1}{2}(v_{i,j} + v_{j,i}) \tag{22}$$

(in Cartesian coordinates), and g_{ij} is the Euclidean metric. Replacing the velocity v by the displacement u and the viscosities by Lamé coefficients gives the elastic solid problem considered above (see A Theory of Harris Wrinkles). A viscoelastic generalization of this problem is solved in Appendix B.

Because the substrate is in the Euclidean plane, there is a canonical identification of it with its tangent space or cotangent space at any point. This freedom to represent geometric objects in several different ways is very useful in computations. A reference on the geometrical methods used here is Schutz (1980). Thinking of v and F as 1-forms, one can write Eq. 20 in coordinate-free form as

$$(\kappa + 2\eta) d * d * v + \eta * d * dv + F = 0, \tag{23}$$

where d is the exterior derivative and $*$ is the Hodge star operator. The velocity v can be represented in terms of potentials

$$v = *d\alpha + d\beta \tag{24}$$

locally for some real functions α and β, so that Eq. 23 becomes

$$(\kappa + 2\eta) d * d * d\beta + \eta * d * d * d\alpha + F = 0. \tag{25}$$

In particular, in the homogeneous case $F = 0$, α and β each solve the biharmonic equation

$$\nabla^2\nabla^2\alpha = \nabla^2\nabla^2\beta = 0. \tag{26}$$

This formulation is coordinate free, but it takes a peculiarly simple form in terms of the complex coordinates z and $\bar{z}$. A comprehensive reference on the complex variable approach and its advantages for boundary value problems is presented by Timoshenko and Goodier (1951). This approach has a very long history, as one sees in references there. I summarize below the results that are needed for the purpose of this paper. It should be emphasized that this approach has great advantages for boundary value problems with geometrically complicated boundaries, as may be expected in biological problems. It is not as familiar in this context as it might be.

It is clear, using

$$\nabla^2 = 4\frac{\partial^2}{\partial z \partial \bar{z}}, \tag{27}$$

that general real solutions to Eq. 26 are

$$\alpha = -2\,\mathrm{Im}(\bar{z}f(z) + g(z)) \tag{28}$$

$$\beta = 2\,\mathrm{Re}(\bar{z}h(z) + j(z)), \tag{29}$$

where f, g, h, and j are arbitrary analytic functions of the complex variable z. Because the representation in Eq. 24 is not unique, it is no loss of generality to take $j = 0$, as I do from now on.

To exploit complex variables most efficiently, it is worthwhile to introduce the notation of Hermitian geometry. If one takes as a basis in the cotangent space the 1-forms dz and $d\bar{z}$, then Euclidean geometry is expressed by the Mermitian metric tensor

$$g(\mathrm{d}z, \mathrm{d}\bar{z}) = g(\mathrm{d}\bar{z}, \mathrm{d}z) = 2. \tag{30}$$

(other components zero). The dual basis in the tangent space is $\partial/\partial z$ and $\partial/\partial\bar{z}$. The Hermitian metric in the tangent space is

$$g\left(\frac{\partial}{\partial z}, \frac{\partial}{\partial \bar{z}}\right) = g\left(\frac{\partial}{\partial \bar{z}}, \frac{\partial}{\partial z}\right) = \frac{1}{2} \tag{31}$$

(other components zero). The action of the Hodge star operator is

$$*\mathrm{d}z = i\,\mathrm{d}z \quad *\mathrm{d}\bar{z} = -i\,\mathrm{d}\bar{z} \tag{32}$$

The identification of the (real) tangent space at any point with the complex plane takes the form

$$A\frac{\partial}{\partial z} + \bar{A}\frac{\partial}{\partial \bar{z}} \leftrightarrow A, \tag{33}$$

and this gives an identification of real tangent fields with complex functions. The identification of the (real) cotangent space at any point with the complex plane takes the form

$$A\,\mathrm{d}z + \bar{A}\,\mathrm{d}\bar{z} \leftrightarrow 2\bar{A}, \tag{34}$$

and this gives an identification of real 1-forms and complex functions. Using this identification together with Eqs. 24, 28, and 32, we have

$$v = 2[z(\bar{h}' - \bar{f}') - \bar{g}' + (f + h)] \tag{35}$$

as a complex function. Still considering the case $F = 0$, one finds from Eq. 25 that

$$\eta f''' = (\kappa + 2\eta)h''. \tag{36}$$

The once integrated form of this relationship

$$\eta f' = (\kappa + 2\eta)h' + c_0, \tag{37}$$

where c_0 is an arbitrary complex constant, is also used below.

The components of the rate-of-strain tensor associated to v are

$$\dot{\sigma}\left(\frac{\partial}{\partial z}, \frac{\partial}{\partial z}\right) = \bar{z}(h'' - f'') - g'' = \overline{\dot{\sigma}\left(\frac{\partial}{\partial \bar{z}}, \frac{\partial}{\partial \bar{z}}\right)} \quad (38)$$

$$\dot{\sigma}\left(\frac{\partial}{\partial z}, \frac{\partial}{\partial \bar{z}}\right) = h' + \bar{h}' = \overline{\dot{\sigma}\left(\frac{\partial}{\partial \bar{z}}, \frac{\partial}{\partial z}\right)}. \quad (39)$$

(One way to compute this is to find the Lie derivative of the metric tensor with respect to v regarded as a tangent vector field.) The divergence of v is the trace of $\dot{\sigma}$ (using g from Eq. 30):

$$v_{i,i} = 4(h' + \bar{h}'). \quad (40)$$

These are the ingredients of the stress tensor Eq. 1.

Now imagine a short directed line segment of length Δl in the direction of $e^{i\theta}$ somewhere in the substrate plane. Using Eqs. 40 and 38, we can find the force exerted on this segment by the substrate to the right of the segment. The unit normal to the segment pointing into this part of the substrate is

$$\hat{n} = -ie^{i\theta}\frac{\partial}{\partial z} + ie^{-\theta}\frac{\partial}{\partial \bar{z}}. \quad (41)$$

The force ΔF on this line segment is found by evaluating the stress tensor on $\hat{n}$, i.e.,

$$\Delta F = S(\hat{n}, \cdot)\Delta l. \quad (42)$$

The result is the real 1-form

$$\Delta F = [2(\kappa + \eta)(h' + \bar{h}')(-i)e^{i\theta}\,d\bar{z} + 2\mu i(z(\bar{h}'' - \bar{f}'') - \bar{g}'')e^{-i\theta}\,d\bar{z} + c.c.]\Delta l, \quad (43)$$

which is also represented by the complex function

$$\Delta F = -4(\kappa + \eta)i(h' + \bar{h}')e^{i\theta}\Delta l + 4\eta i[z(\bar{h}'' - \bar{f}'') - \bar{g}'']e^{-i\theta}\Delta l, \quad (44)$$

using the identification Eq. 34. When we integrate over a curve, thought of as made up of many such segments, $e^{i\theta}\Delta l$ becomes dz, and $e^{-i\theta}\Delta l$ becomes $d\bar{z}$. Thus the force on a directed curve C due to the substrate material to its right is

$$F_{sub} = 4\eta i\int_C [z(\bar{h}'' - \bar{f}'') - \bar{g}'']\,d\bar{z} - 4i(\kappa + \eta)\cdot\int_C (h' + \bar{h}')\,dz. \quad (45)$$

Using Eq. 37, this becomes

$$F_{sub} = 4\eta i\int_C d[z(\bar{h}' - \bar{f}') - \bar{g}' - (1 + \kappa/\eta)h + c_0 z], \quad (46)$$

the integral of a total derivative. In particular, if C is a closed curve,

$$F_{sub} = 4\eta i[z(\bar{h}' - \bar{f}') - \bar{g}' - (1 + \kappa/\eta)h], \quad (47)$$

where the square brackets [ ] mean the jump in the enclosed function at a presumed cut. Now using Eq. 36 and the fact that u is single valued, implying, according to Eq. 35,

$$[z(\bar{h}' - \bar{f}') - \bar{g}'] = -[f + h], \quad (48)$$

we find the very simple result

$$F_{sub} = -8\eta i\,[f]. \quad (49)$$

Of course, if f is single valued (has no cut), then according to Eq. 49 the substrate force is zero. This is to be expected, because we have been solving the homogeneous version of Eq. 2. In equilibrium the net force on each piece of the substrate is zero, and f is a regular function in the interior of C.

In a similar way we can find the net torque exerted on the curve C with respect to the origin by the substrate material on its right. It is

$$\tau_{sub} = 4\eta\,\mathrm{Re}\int_C \bar{z}\,d[z(\bar{h}' - \bar{f}') - \bar{g}' - (1 + \kappa/\eta)h + c_0 z] \quad (50)$$

$$= 4\eta\,\mathrm{Re}\int_C d[\bar{z}z(\bar{h}' - \bar{f}') - z\overline{g}' + g], \quad (51)$$

where in the second line we used Eq. 37 and added a purely imaginary term to the integrand. This is once again the integral of a total derivative. The integral around a closed curve, using again Eq. 48, is the discontinuity at a cut,

$$\tau_{sub} = -4\eta\,\mathrm{Re}[\bar{z}(f + h) - g]. \quad (52)$$

Of course, if the functions f, g, and h are single valued, there is no substrate torque, as would be expected in equilibrium.

To this point I have only solved the homogeneous problem, with external forces applied perhaps on the boundary, but the above observations also solve the inhomogeneous problem. If a small piece of the substrate is subject to an external force, then in equilibrium the adjoining substrate must exert a force to balance the external force—this is the content of Eq. 20. By Eq. 49 this means f must have a logarithmic singularity at this point. At the same time, there cannot be a singularity in the torque at a point, and this condition determines the singularity of g. (Alternatively, Eq. 48 determines this singularity.) Additional nonsingular terms can be added to f and g, leading to a whole family of Green's function solutions, parameterized by two analytic functions. This is enough freedom to fix u on the boundaries of a finite region, for example, so it corresponds exactly to intuition. We thus have the following singular solution, with a nonsingular term added in g to facilitate comparison with the classical solution to this problem cited in (Dembo et al., 1996):

$$f = c\ln z \quad (53)$$

$$g = -\frac{3\eta + \kappa}{2\eta + \kappa}\bar{c}z\ln z + \frac{2\eta}{2\eta + \kappa}\bar{c}z \quad (54)$$

$$h = \frac{c}{2\eta + \kappa}\ln z, \quad (55)$$

where c is a complex constant. The force applied by the substrate to any region containing the origin is, by Eqs. 49 and 53,

$$F_{sub} = 16c\pi\eta. \quad (56)$$

Equating this to $-F_{ext}$ determines

$$c = -\frac{F_{ext}}{16\pi\eta}. \tag{57}$$

Then using Eqs. 35, 53, 54, 55, and 57, we have the velocity v in response to the force F_{ext} applied at the origin:

$$v = -\frac{1}{4\pi\eta}\left[\left(\frac{\kappa+3\eta}{\kappa+2\eta}\right)F_{ext}\ln|z| + i\left(\frac{\kappa+\eta}{\kappa+2\eta}\right)\frac{\mathrm{Im}(\bar{z}F_{ext})}{\bar{z}}\right], \tag{58}$$

and Eq. 13 follows.

B: Viscoelastic model

In this section I point out a simple viscoelastic generalization of the model in Appendix A, and describe how it fails to improve the fit to keratocyte data on a fluid substrate. Suppose that the two-dimensional fluid has a "memory," so that stress at any time depends on the rate of strain not only at that time but also in the past. This viscoelastic stress Σ_{ij} can be represented in terms of the stress S_{ij}, which would exist in a simple fluid by (Bird et al., 1987)

$$\Sigma_{ij} = \int_{-\infty}^{t} G(t-t')S_{ij}\,dt', \tag{59}$$

where G is the relaxation function. (My conventions differ from those used by Bird et al. by a factor of 2 in the strain tensor and a minus sign in the stress tensor.) Typically G falls off with time, meaning that strain in the distant past has relaxed and cannot contribute to stress in the present. Although the form is more general, I shall take G to be characterized by a single exponential memory time τ, the so-called Maxwell model, for simplicity. The reason is that I am not trying to give a realistic description of viscoelastic substrates, for which there is not even any evidence, but only trying to detect any hint of elasticity in observed substrates. The Maxwell model says Eq. 59 is the solution of

$$\Sigma + \tau\frac{\partial\Sigma}{\partial t} = S. \tag{60}$$

The mechanical equilibrium of the viscoelastic fluid is expressed by

$$\Sigma_{ij,j} = -F_i^{ext}, \tag{61}$$

where $\vec{F}^{ext}$ is the force per unit area applied to the substrate by the cell in the contact area D. Because Σ is found by integrating spatial derivatives of the velocity V, Eq. 61 is best thought of as an integro-differential equation for the velocity $\vec{V}$ that results from the application of the external force $\vec{F}^{ext}$.

Except for the appearance of the relaxation function G, Eq. 61 is just the equation for the velocity field of a two-dimensional fluid subject to an external force F. The solution is therefore (see Appendix A)

$$\int_{-\infty}^{t} G(t-t')V(z,t')\,dt' = -\frac{1}{4\pi\eta}\iint_D\left[a_3F\ln|z-w| + ia_1\frac{\mathrm{Im}[F(\bar{z}-\bar{w})]}{\bar{z}-\bar{w}}\right]dA_w, \tag{62}$$

where D is the region over which the force F is applied, i.e., the contact area of the cell, and

$$a_1 = \frac{\kappa+\eta}{\kappa+2\eta} \tag{63}$$

$$a_3 = \frac{\kappa+3\eta}{\kappa+2\eta}. \tag{64}$$

Then, inverting the linear operator on the left, as in Eq. 60, we have

$$V(z,t) = -\left(1+\tau\frac{\partial}{\partial t}\right)\frac{1}{4\pi\eta}\iint_D\left[a_3F\ln|z-w| + ia_1\frac{\mathrm{Im}[F(\bar{z}-\bar{w})]}{\bar{z}-\bar{w}}\right]dA_w. \tag{65}$$

It was pointed out in Eq. 7 that for the keratocyte experiment analyzed above (Data Analysis), the time-dependent velocity V of the substrate in the laboratory frame has the form

$$V(z,t) = v(x - v_0t, y), \tag{66}$$

where v_0 is the constant speed of the cell, and the function $v(x, y)$ is a steady flow velocity in the cell frame, due to an assumed constant distribution of force F. From the way V depends on t it follows that on the right side of Eq. 65 the operator $\partial/\partial t$ can be replaced by $-v_0\partial/\partial x$. Thus the steady flow pattern is

$$v(z) = -\frac{1}{4\pi\eta}\iint_D\left[a_3F\ln|z-w| + ia_1\frac{\mathrm{Im}[F(\bar{z}-\bar{w})]}{\bar{z}-\bar{w}}\right]dA_w + \frac{v_0\tau}{4\pi\eta}\iint_D\left[a_3F\frac{\mathrm{Re}(z-w)}{|z-w|^2} + ia_1\bar{F}\frac{\mathrm{Im}(z-w)}{(\bar{z}-\bar{w})^2}\right]dA_w. \tag{67}$$

If $\tau = 0$, this relationship between external force F and v reduces to that of Appendix A (the memory fluid has no memory—it reduces to a simple fluid). For positive τ one gets a family of models parameterized by memory time. The data above (Data Analysis) were fit with these models using τ as a parameter. The best fits were for τ smaller than the time the experiment could resolve. That is, the extra degree of freedom in the fitting function led to no improvement in fit. There was no indication of elasticity in the substrate.

C: Three-dimensional fluid model

A classical application of Green's identity to the problem of low Reynold's number fluid flow is Oseen's integral representation (Oseen, 1927) for the three-dimensional creeping flow of a fluid with shear viscosity η in an open bounded region D in terms of boundary data on the smooth boundary M,

$$v_k(\vec{r}_0) = \frac{1}{8\pi\eta}\iint_M\left[t_{jk}\left(\eta\frac{dv_j}{dn} - Pn_j\right) - v_j\left(\eta\frac{dt_{jk}}{dn} - p_kn_j\right)\right]d^2\vec{r}. \tag{68}$$

Here $\vec{r}_0$ is a fixed (interior) point of D, and j and k are indices running from 1 to 3, labeling Cartesian components of several vectors and

tensors. The vector with components n_j is the unit outer normal $\hat{n}$ on M. The derivative d/dn is best understood as minus the partial derivative in the direction $-\hat{n}$, because it is not clear from this representation that the flow exists outside of D. The tensor t_{jk} and the vector p_k should be thought of as known quantities, depending on the variable of integration $\vec{r}$ and the parameter $\vec{r}_0$. They are three Stokes flows (labeled by k) with a Green's function singularity at $\vec{r} = \vec{r}_0$, and may be taken to be (Oseen, 1927)

$$t_{jk}(\vec{r}, \vec{r}_0) = \frac{\delta_{jk}}{|\vec{r} - \vec{r}_0|} + \frac{(x_j - x_{0j})(x_k - x_{0k})}{|\vec{r} - \vec{r}_0|^3} \tag{69}$$

$$p_k(\vec{r}, \vec{r}_0) = 2\eta \frac{(x_k - x_{0k})}{|\vec{r} - \vec{r}_0|^3}. \tag{70}$$

Here x_j is a Cartesian component of $\vec{r}$, etc.

Suppose an isotropic three-dimensional Newtonian fluid with shear viscosity η_3 fills the half-space given by $z \leq 0$, and that small tractions are applied tangentially on some finite region of the boundary M given by $z = 0$. The integral representation Eq. 68 contains as a special case the motion of the plane fluid interface in response to these tractions. (It is clear that this represents a possible model of the Jacobson-Oliver experiment.) Let the point $\vec{r}_0$ approach the boundary M. The integral representation becomes

$$v_k(\vec{r}_0) = \frac{1}{4\pi\eta_3} \iint_M \eta_3 \frac{dv_j}{dn} t_{jk} d^2\vec{r}. \tag{71}$$

This limit is discussed by Peterson (1996). The quantity $\eta_3(dv_j/dn)$ is just the negative of the shear stress traction applied by the underlying fluid on the boundary. Because the net force on the boundary must vanish, it is also exactly the traction F_j being applied externally. Thus Eq. 71 is a formula like those in Appendices A and B, giving the velocity of the surface in terms of applied tractions. To put it in exactly the same form, introduce the complex coordinate z in M (not to be confused with the Cartesian coordinate defining M)

$$v(z) = \frac{1}{4\pi\eta_3} \iint_D \left[\frac{3}{2} \frac{F}{|z - 2|} + \frac{1}{2} \frac{\bar{F}(z - w)^2}{|z - w|^3} \right] dw. \tag{72}$$

This is a model that regards the surface as the structureless plane boundary of an isotropic three-dimensional fluid. As noted in the Introduction, it is not possible to choose F's to fit the observed v's with the same goodness of fit as is achieved by the two-dimensional model of Appendix A. This suggests that the fluid near the surface is not inherently isotropic, or that it is not free of internal (two-dimensional) stress, or both.

As in Appendix B, we can form models that are linear combinations of this model, representing the effect of stress from the underlying layer, and the model of Appendix A, representing stress within the surface layer. The result, as in Appendix B, is that the new terms, in this case representing bulk effects, do not improve the fit, and the best fit is obtained when they are negligible.

D: Stress tensor

With the notation of Appendix A, the stress tensor in a two-dimensional solid film with Lamé constants λ and μ has the form

$$S = \begin{pmatrix} a & b \\ b & \bar{a} \end{pmatrix}, \tag{73}$$

where

$$a = S\left(\frac{\partial}{\partial z}, \frac{\partial}{\partial z} \right) = 2\mu[\bar{z}(h'' - f'') - g''] \tag{74}$$

$$b = S\left(\frac{\partial}{\partial z}, \frac{\partial}{\partial \bar{z}} \right) = 2(\lambda + \mu)(h' + \bar{h}'). \tag{75}$$

(Note b is real.) The parabolic points occur where the determinant vanishes, i.e., where

$$|a| = |b|. \tag{76}$$

Evaluating S on a unit vector $\hat{n}$ in the direction θ gives

$$S(\hat{n}, \hat{n}) = 2[\mathrm{Re}(e^{2i\theta}a) + b]. \tag{77}$$

The hyperbolic regions are those where there are two distinct directions (null directions) which make this quantity zero, which is possible only if $|b| < |a|$. The two characteristic directions are the directions perpendicular to these two null directions. At a parabolic point the characteristic directions degenerate to a single characteristic direction given by

$$\theta = \frac{1}{2} Arg\left(\frac{b}{a} \right) \tag{78}$$

If one asks for eigenvectors of S, one is thinking of S as a map of the tangent space to itself, which is really

$$gS = \begin{pmatrix} 0 & 2 \\ 2 & 0 \end{pmatrix} \begin{pmatrix} a & b \\ b & \bar{a} \end{pmatrix} = 2 \begin{pmatrix} b & \bar{a} \\ a & b \end{pmatrix}, \tag{79}$$

where g, the Hermitian metric (Eq. 30), maps cotangent vectors to tangent vectors. It is easy to check that at a parabolic point the nonzero eigenvalue is $4b$ and so has the sign of b (i.e., if $b > 0$, the point is a P-parabolic point, and if $b < 0$, it is an N-parabolic point, in the language used above (see A Theory of Harris Wrinkles).

More generally, the eigenvalues of the stress tensor are

$$\sigma_\pm = 2(b \pm |a|), \tag{80}$$

and the corresponding eigenvectors are in the directions

$$-Arg(\pm a)/2. \tag{81}$$

The stress tensor due to a force F concentrated at the origin can be found from Eqs. 74–75, using the functions f, g, and h from Eqs. 53–55, but with the viscosities κ and η replaced by Lamé constants λ and μ. The result is

$$a = -\frac{1}{4\pi} \left[\frac{\mathrm{Re}(\bar{z}F)}{z^2} + i \frac{\mu}{\lambda + 2\mu} \frac{\mathrm{Im}(z\bar{F})}{z^2} \right] \tag{82}$$

$$b = -\frac{1}{4\pi} \frac{\lambda + \mu}{\lambda + 2\mu} \frac{\mathrm{Re}(\bar{z}F)}{|z|^2}. \tag{83}$$

The stress due to a superposition of forces at different points follows straightforwardly from this. This is the method for constructing Fig. 6, which used the limit $\lambda \to \infty$, corresponding to an incompressible film.

A real force (i.e., pointing in the $+x$ direction) at the origin gives rise to a stress tensor at $z = re^{i\theta}$ with

$$a = -\frac{F}{4\pi r} e^{-2i\theta} \left[\cos\theta + i \frac{\mu}{\lambda + 2\mu} \sin\theta \right] \tag{84}$$

$$b = -\frac{F}{4\pi r} \frac{\lambda + \mu}{\lambda + 2\mu} \cos\theta. \tag{85}$$

One sees from the remark after Eq. 77 that all points are hyperbolic, except in the limiting case $\lambda \to \infty$, in which all points become parabolic. In this case, because of the sign of $\cos\theta$, which determines the sign of b, they are all N-parabolic for $x > 0$ and P-parabolic for $x < 0$. The characteristic direction according to Eq. 78 is θ (i.e., radial), as asserted above (see A Theory of Harris Wrinkles). The tension directions are then along rays from the origin for $x < 0$, corresponding to familiarly observed wrinkles.

I would like to thank Prof. Erich Sackmann for hospitality while this work was begun. I am grateful to Ken Jacobson and Tim Oliver for many conversations, and for sending me their original data. I am especially grateful to Rachel Fink for introducing me to this problem, for helpful conversations along the way, and for material help in transferring and converting data. I thank Morana Lasic for discussions about keratocytes, and for permission to use her picture in Fig. 7. I thank an anonymous referee for drawing my attention to tension field theory. Finally I thank Barbara Danowski for showing me real Harris wrinkles.

REFERENCES

Bird, R. B., R. C. Armstrong, and O. Hassager. 1987. Dynamics of Polymeric Liquids, 2nd Ed., Vol. 1. John Wiley and Sons, New York.

Courant, R., and D. Hilbert. 1962. Methods of Mathematical Physics, Vol. 2. John Wiley and Sons, New York.

Dembo, M., T. Oliver, A. Ishihara, and K. Jacobson. 1996. Imaging the traction stresses exerted by locomoting cells with the elastic substratum method. *Biophys. J.* 70:2008–2022.

Euteneuer, U., and M. Schliwa. 1984. Persistent directional motility of cells and cytoplasmic fragments in the absence of microtubules. *Nature.* 310:58–61.

Fink, R. D., editor. 1995. CELLebration. Video. 37 min. Sinauer Associates, Sunderland, MA.

Garabedian, P. R. 1964. Partial Differential Equations. John Wiley and Sons, New York.

Harris, A. K., D. Stopak, and P. Wild. 1980. Silica rubber substrate: a new wrinkle in the study of cell locomotion. *Science.* 208:177–179.

Lamb, H. 1945. Article 341. *In* Hydrodynamics, 6th ed. Dover Publications, New York.

Landau, L. D., and E. M. Lifshitz. 1959. Theory of Elasticity. Addison-Wesley, Reading, MA.

Lasic, M. 1994. Cultured cell migration on glass, collagen, and silicone rubber substrata. Undergraduate senior thesis. Mount Holyoke College, South Hadley, MA.

Mansfield, E. H. 1969. Tension field theory. *In* Proceedings of the Twelfth International Congress of Applied Mechanics. Springer-Verlag, Berlin. 305–320.

Oliver, T. N., J. Lee, and K. Jacobson. 1994. Forces exerted by locomoting cells. *Semin. Cell Biol.* 5:139–147.

Oliver, T., M. Leonard, J. Lee, A. Ihihara, and K. Jacobson. 1993. Video microscopic measurement of cell-substratum traction forces generated by locomotory keratocytes. *In* Proceedings of the 51st Annual Meeting of the Microscopy Society of America. San Francisco Press, San Francisco.

Oseen, C. W. 1927. Hydrodynamik. Leipzig.

Peterson, M. A. 1996. Membrane hydrodynamics at low Reynolds number. *Phys. Rev.* E53:731–736.

Reissner, E. 1938. On tension field theory. Proceedings of the Fifth International Congress on Applied Mechanics.

Schutz, B. 1980. Geometrical Methods of Mathematical Physics. Cambridge University Press, Cambridge.

Timoshenko, S., and J. N. Goodier. 1951. Theory of Elasticity, 2nd Ed. McGraw-Hill, New York.

Wagner, H. 1929. *Z. Flugtechnol. Motorluftschiffahrt.*